SUPPLEMENTAL MATERIALS

Supplemental Figure S1

Mouse models for two types of human hereditary deafness with Cx26 mutations.

(**A**) The construction of the transgene vector containing human Cx26 with dominant-negative R75W mutation for the transgenic ($Cx26^{R75W+}$) mouse. (**B**) Enhanced green fluorescent protein (EGFP) expression in a neonatal transgenic mouse (left pup) as an indicator of transgene expression. The pup on the right is a non-transgenic littermate. (C) Generation of the Cx26 conditional knockout mouse ($Cx26^{f/f}$P0Cre) was achieved by constructing a targeting vector with a floxed coding sequence for all of Cx26 (filled box) with loxP sequences (triangles) and the neomycin resistance gene (neo). The vector was designed to produce a null allele in the mouse after Cre enzyme application. $Cx26^{f/f}$P0Cre mice were produced as described in the Materials and Methods to delete the coding sequence of the Cx26 gene in neural crest–derived cells, which include the inner ear tissue. IRES; internal ribosomal entry site. B; BamHI. RI; EcoRI. H; HindIII. Sc; SacI, DT-A (Diphtheria toxin A). (**D**) Recording of the auditory brainstem response (ABR) in 7-w-old $Cx26^{f/f}$P0Cre mice as compared with their littermate controls ($Cx26^{f/f}$) from three litters (n = 7, mean ± SE with dot plots) showed a significant threshold shift in $Cx26^{f/f}$P0Cre mice for both 8 kHz ($P = 3.6 \times 10^{-9}$) and 20 kHz ($P = 2.2 \times 10^{-6}$). ***, P <0.001**.** The maximum output level was 93.5 and 83.4 dB at 8 and 20 kHz, respectively; 5 dB were added to these values when the ABR was not detected even at the maximum output.

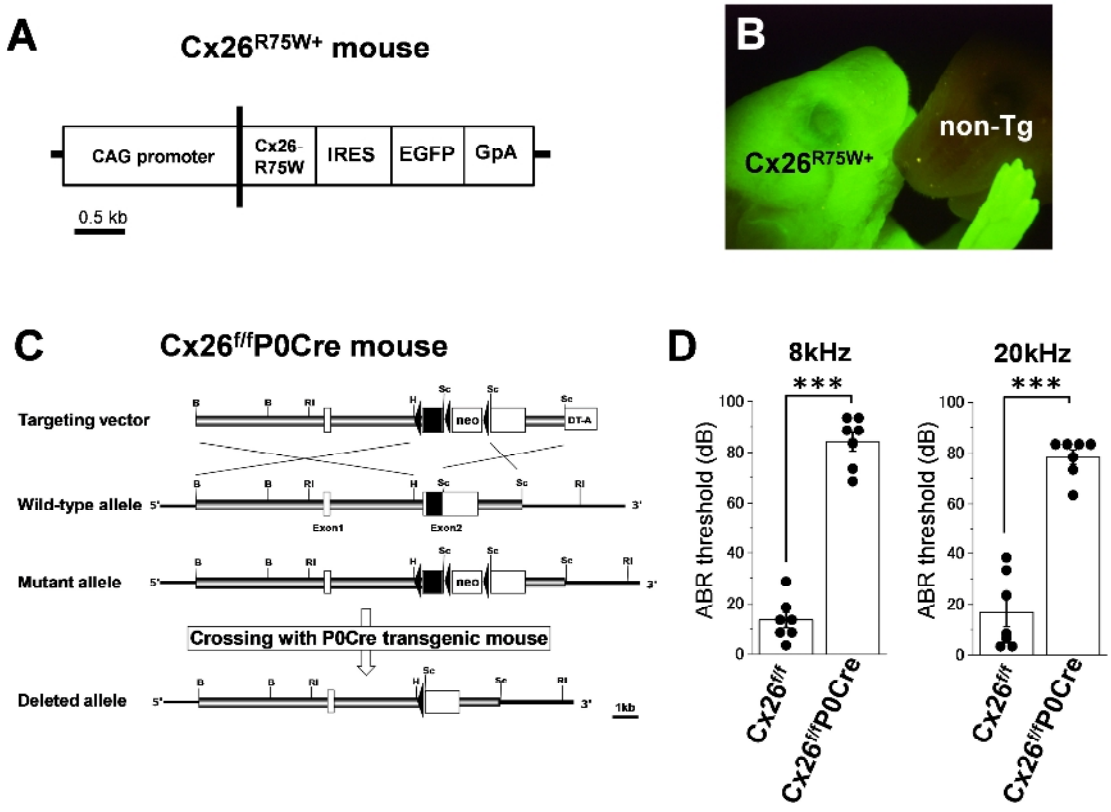

Supplemental Figure S2

Cre recombinase expression in P0-Cre mice crossed with ROSA26-GFP reporter mice.

(**A**,**B**) Whole-mount observation of the E10.5 mice with the normal (**B**) and stereoscopic (**A**) fluorescence microscope showing GFP signals in the inner ear lineage region and the otic vesicle (OV) with the ganglia of VII and VIII (VII/VIII). (**C**–**E**) Immunolabeled cryosections with anti-GFP were observed with confocal microscopy. Sagittal (**C**) and transverse (**D**) sections showed strong Cre recombinase expression in OV and VII/VIII. (**E**) High-magnification image of OV from **D** showed that most of the cells had strong Cre recombinase expression. Nuclei were counterstained with DAPI (blue). Bars indicate 500 μm for **A**,**B** and 50 μm for **C**–**E**. NT, neural tube.

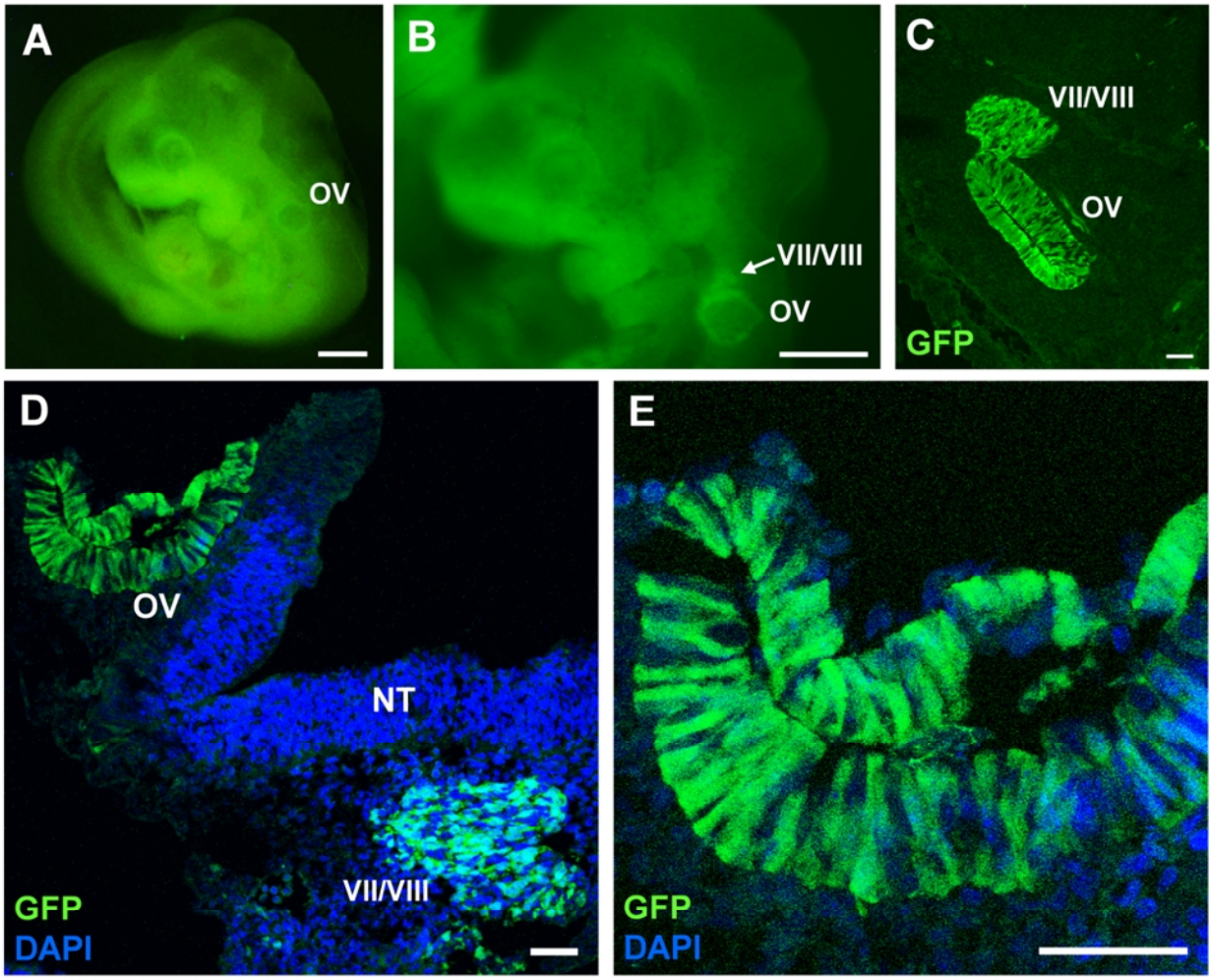

Supplemental Figure S3

Spontaneous Ca^{2+} signaling is affected in the $Cx26^{f/f}$P0Cre cochlea.

(**A**,**C**) Cochlear tissues were dissected and loaded with the Ca^{2+} reporter fluo-4 AM and imaged for 7 min at 2 frames/s. (**B**,**D**) The line scale images obtained from the regions indicated in **a** and **c** represent the frequency and propagation of the spontaneous Ca^{2+} signaling wave during 7 min. Crucial differences in the Ca^{2+} signal propagation (double-headed arrow) were observed between $Cx26^{f/f}$P0Cre and the control littermate. (**E**) The propagation range (mean ±S.E., n=9) was significantly decreased (***; $P = 0.0007$) in cochleae from $Cx26^{f/f}$P0Cre mice. Bars in **A** and **C** indicate 100 µm.

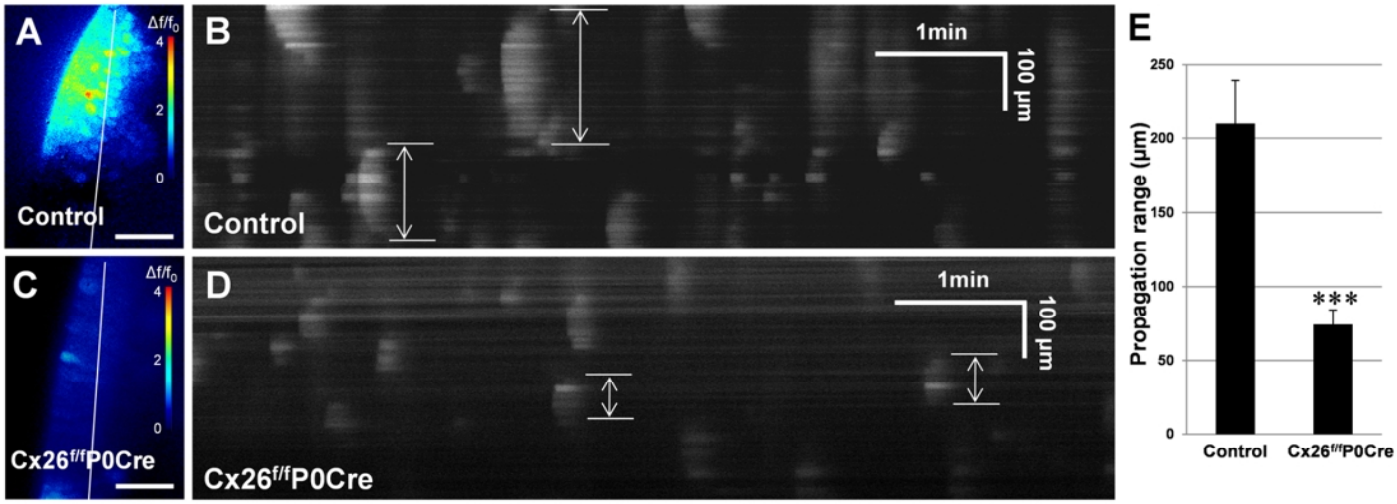

Supplemental Figure S4

Reduced plaque formation at the initial forming stage (E14.5) of normal cochlear GJPs with Cx30 in the two Cx26 mutant mouse lines.

(**A**–**D**) Whole-mount cochlear tissue was immunolabeled with anti-Cx30 to compare the initial GJP formation. $Cx26^{R75W+}$ (**B**) and $Cx26^{f/f}$P0Cre (**D**) showed notably reduced GJP formation, although the control (**A**, non-Tg littermate of $Cx26^{R75W+}$ and **C**, $Cx26^{f/f}$) formed a number of large GJPs (L-GJPs, brackets) within the small-GJPs (S-GJPs) at this stage. In mice from both mutant lines, only S-GJPs were infrequently observed within the region that would become ISCs. Bars indicate 5 μm. (**E**) The length of the largest GJP along a single cell border was compared among control, $Cx26^{R75W+}$ and $Cx26^{f/f}$P0Cre mice (mean ± SE, n = 21 for all four groups). The GJP length in the mutant mice was significantly smaller than that in their corresponding controls. ***$P = 6.3 \times 10^{-5}$ and 6.5×10^{-5} for $Cx26^{R75W+}$ and $Cx26^{f/f}$P0Cre, respectively, relative to the control (Student's t-test).

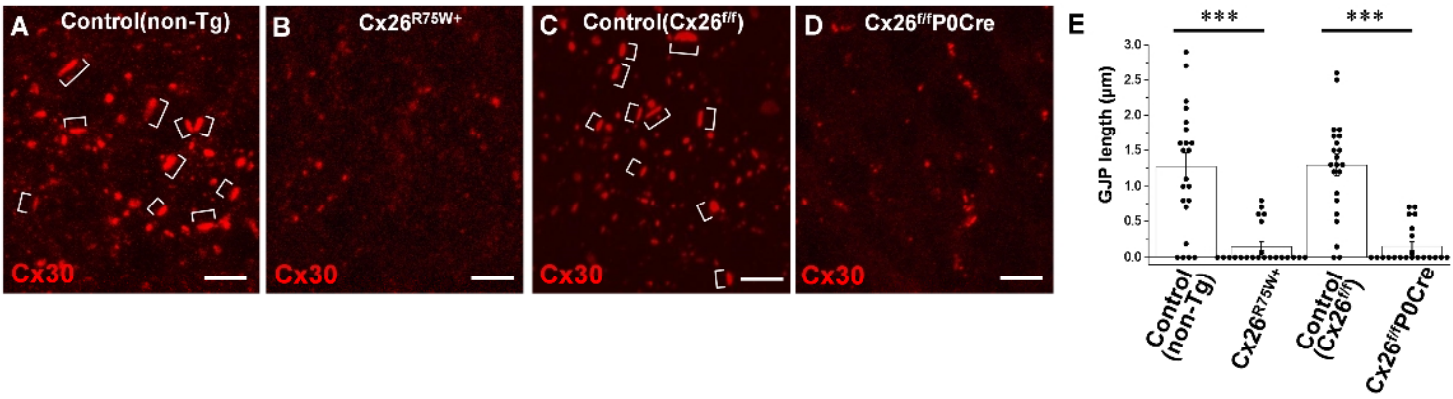

Supplemental Figure S5

GJP formation in postnatal development of the cochlea.

The ISCs at P5 showed the disruption of GJPs that is present in adult mice. (**A**–**C**) Conformational changes in GJPs shown by Cx30 immunolabeling. Severe GJP disruptions were observed in $Cx26^{f/f}$P0Cre mice (**C**). In contrast, the littermate of $Cx26^{R75W+}$ (**A**, non-Tg) showed the large flat GJPs as adult control mice at this stage. Although GJP disruption in $Cx26^{R75W+}$ mice was not as severe as that in $Cx26^{f/f}$P0Cre mice (**C**), plaque disassembly as indicated by gaps in the plaques (**B**, arrows in inset) was frequently observed in ISCs of $Cx26^{R75W+}$ mice. (**D**–**F**) Double immunolabeling of Cx26 and Cx30 in ISCs from control and $Cx26^{f/f}$P0Cre mice. (**D**) In control mice, a small number of S-GJPs with only Cx30 were observed (arrowheads), although most of the GJPs were L-GJPs with both Cx26 and Cx30 (arrows). (**E**,**F**) Cx26/Cx30-positive L-GJPs (arrow) were occasionally observed even in $Cx26^{f/f}$PCre mice because of the cellular mosaicism shown in **Figure 1K-O**. On the other hand, most of the other GJPs without Cx26 formed S-GJPs (arrowheads) with drastically reduced plaque areas. The inner hair cells (IHC) were shown to indicate the localization and the orientation of ISCs in the images. Bars indicate 5μm.

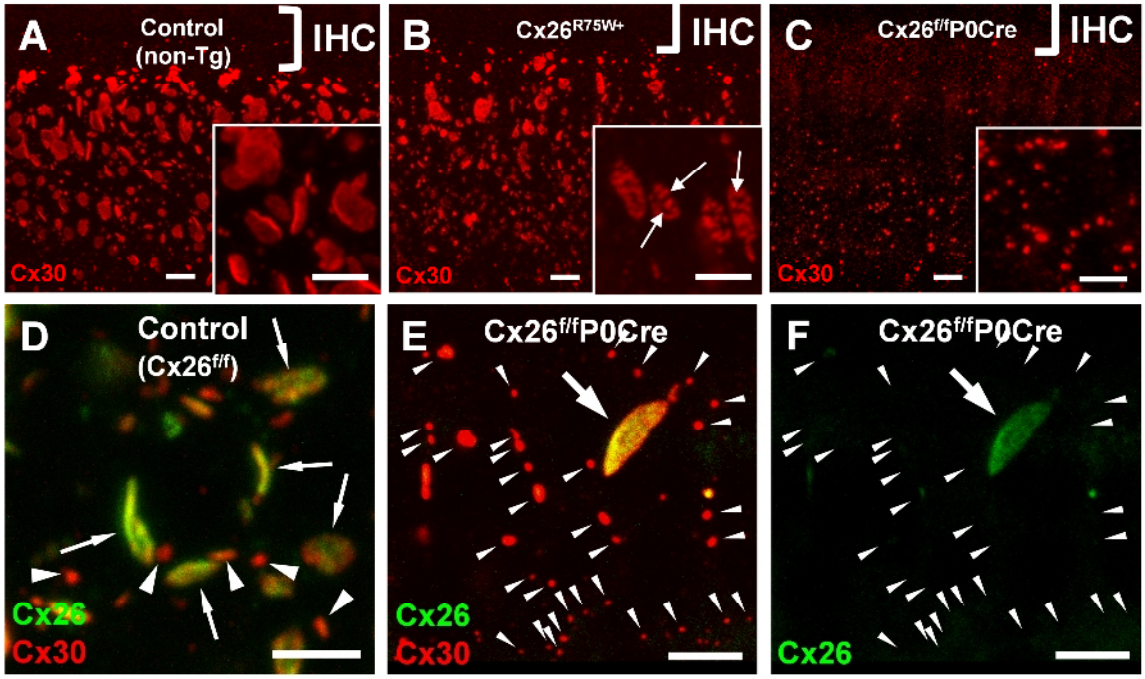

Supplemental Figure S6

Exogenous overexpression of Cx26 in organotypic cultures transduced with AAV-Cx26-FLAG leads to the formation of large GJPs in Cx26-deficient mice (Cx26$^{f/f}$P0Cre) but not in mice with the dominant-negative (Cx26^{R75W+}) mutation.

Cochlear organotypic cultures from 6-w-old Cx26^{R75W+} (**A**) and Cx26$^{f/f}$P0Cre (**B**) mice were used for gene transfer with AAV-Cx26-FLAG. *z*-stack images of immunolabeled FLAG (red) were obtained by confocal microscopy. Bars indicate 10 µm. (**C**) The length of the largest GJP as shown by Cx26-FLAG labeling along 6 cell borders in ISCs from four mice (n = 24) was compared between Cx26^{R75W+} and Cx26$^{f/f}$P0Cre mice (dot plot with mean ± SE). Cx26$^{f/f}$P0Cre showed many large (>5 µm) GJPs with Cx26-FLAG (**B**, arrows) and the GJP lengths were significantly longer than those from Cx26^{R75W+} mice,as determined by the Student's *t*-test. ***P = 0.00022

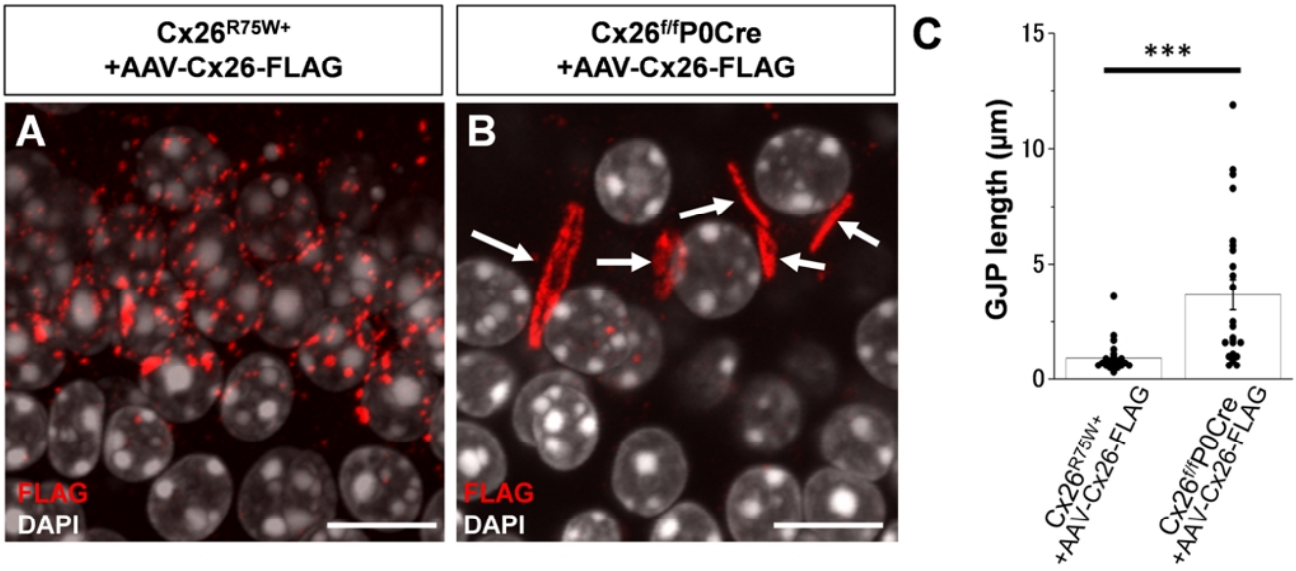

Supplemental Figure S7

Immunoblot analysis of the proteins associated with endocytosis and assembly of membrane protein complexes in cochleae from Cx26^{R75W+} mice.

(**A**,**B**) There were no notable changes in the expression of Myosin6 (MYO6) and Clathrin light chain B (CLTB) at 2 w and 8 w (**A**) or of Vinculin and Talin at 8 w (**B**). CLTB expression, which is an indicator of clathrin-dependent endocytosis, was not upregulated, although the expression of caveolins, which are indicators of caveolin-dependent endocytosis, was upregulated (**Fig. 5A-D**). Control, control littermates of Cx26^{R75W+} mice.

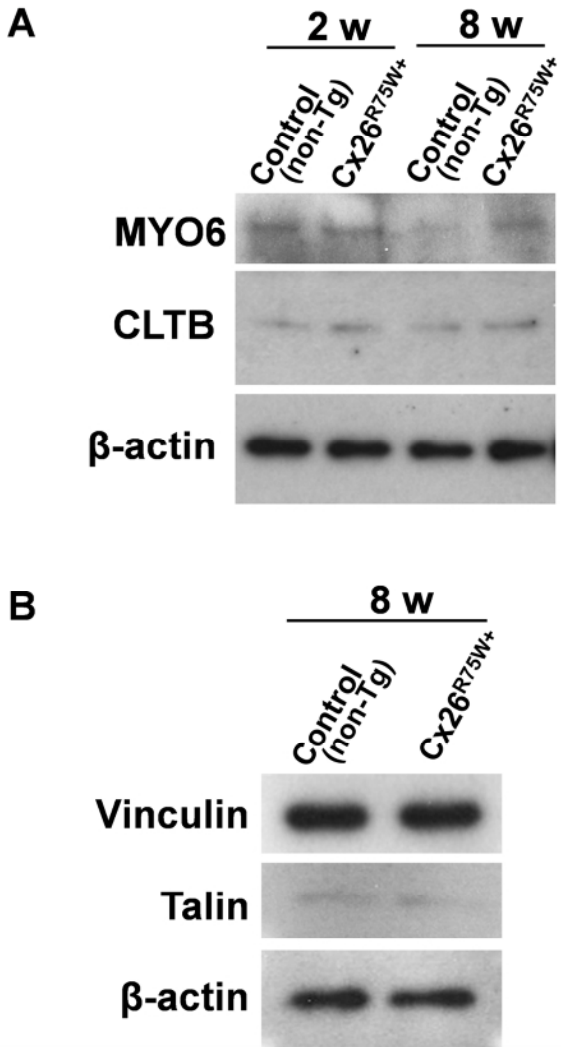

Supplemental Figure S8

Accumulated CAV1β around Cx26 R75W and Cx30.

GFP tagged with human wild-type Cx26 (**A**, Cx26-GFP), Cx26-R75W (**B**, Cx26^{R75W}GFP) or Cx30 (**C**, Cx30-GFP) expression plasmids were co-transfected with a plasmid that expressed human CAV1β tagged with V5 (red, CAV1β-V5) in HEK293 cells. Insets show high-magnification images of boxed areas. In Cx26-R75W (**B**) and Cx30 (**C**), a number of GJPs at cell borders and the connexin vesicles were accompanied by accumulated CAV1β-V5 (arrowheads and asterisks, respectively), although wild-type Cx26 with CAV1β-V5 (**A**) did not show such a distribution pattern. Scale bars: 10 μm and insets: 2.5 μm.

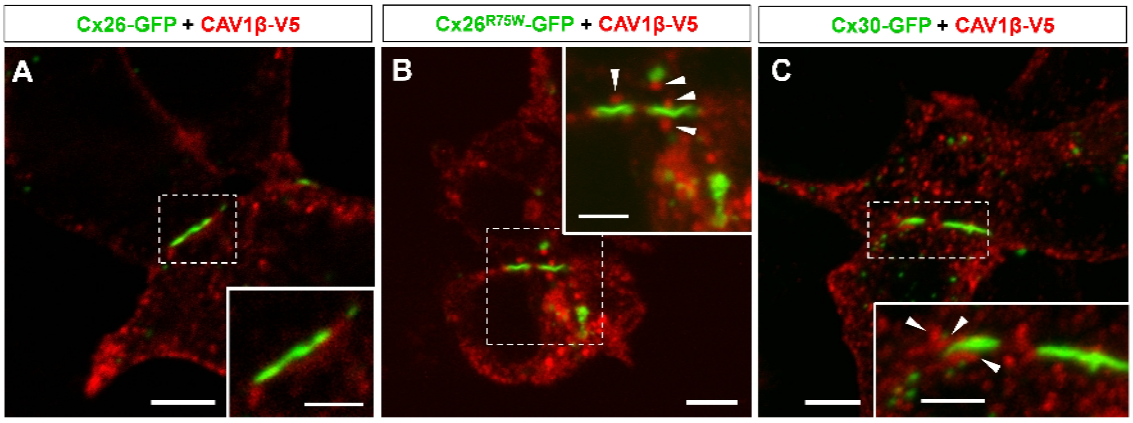

Supplemental Figure S9

Lipid raft distribution is partially affected around disrupted GJPs in Cx26$^{f/f}$P0Cre.

(**A, B**) Immunolabeling of caveolins and lipid raft labeling in ISCs of littermate control (Cx26$^{f/f}$) and Cx26$^{f/f}$P0Cre adult (8 w) mice. The images from **Figure 4G**,**H** labeled Cx30 (blue) and Caveolin1 (green) overlaid with staining for cholera toxin B (CTxB, red), which labels lipid rafts. (**C,D**) Association between GJP and lipid raft were shown in littermate control (Cx26$^{f/f}$, **C**) and Cx26f/fP0Cre (**D**) cochlea. Distinct lipid rafts were observed mainly at the gaps between GJPs in littermate control (brackets in A and arrowheads in **C**). In Cx26f/fP0Cre mice (**D**), a part of the lipid raft signals showed more-diffuse and irregular distribution (**D**, brackets), as compared with those from the control (**C**). (**E,F**) Schematic diagrams showing the localization of GJPs (blue), caveolins (green) and lipid rafts (red) in control (**E**) and Cx26 mutant (**F**) cochleae. Bars indicate 5 μm.

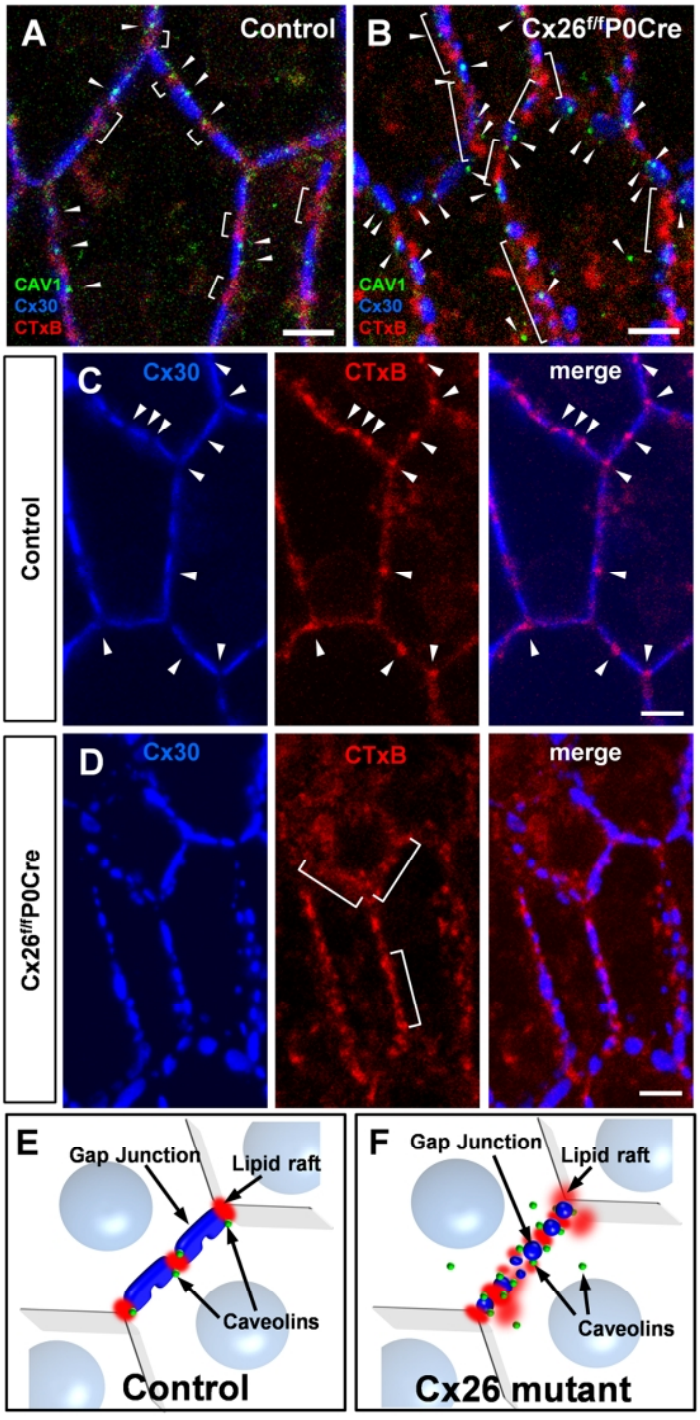

Supplemental Figure S10

Protein distribution and association between cochlear connexins.

(**A**) Immunoblot analysis of the cytoplasmic (C) fraction and plasma membrane (M) fraction from the cochlea of a $Cx26^{R75W+}$ mouse and littermate control. Cx26 and Cx30 proteins in $Cx26^{R75W+}$ mice were properly distributed in the plasma membrane. (**B**) Co-immunoprecipitation assay with anti-Cx26. Cx26 and Cx30 proteins were properly immunoprecipitated (IP) with anti-Cx26 from isolated cochlear proteins that included those from the lateral wall and the organ of Corti from $Cx26^{R75W+}$ mice as well as from littermate control. Proteins were detected by western blotting (WB) with the indicated antibodies.

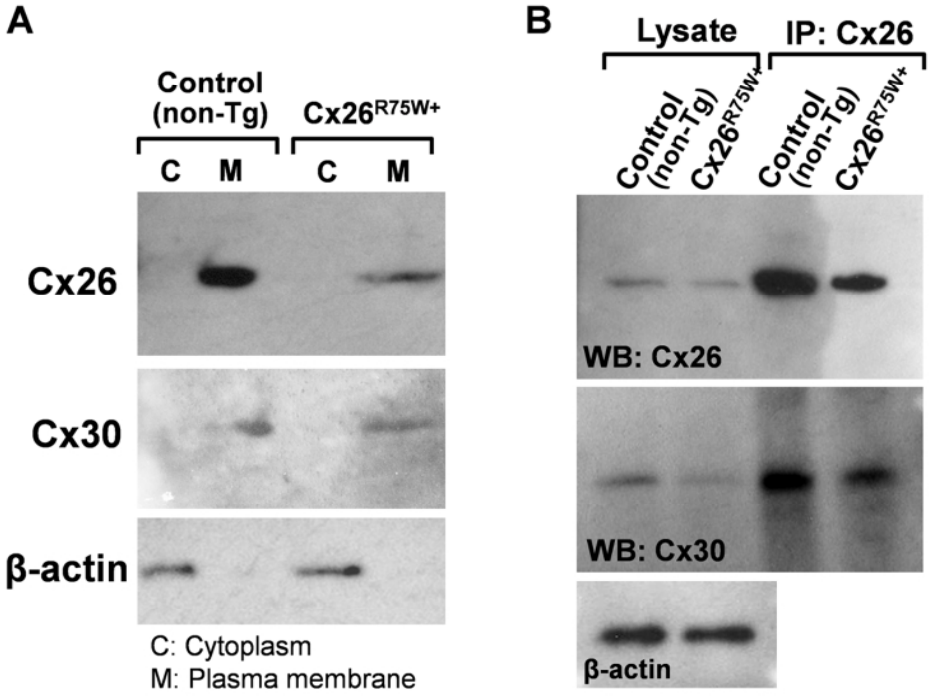

SUPPLEMENTARY VIDEO LEGENDS

Supplemental Video 1

Three-dimensional video images of GJPs in a 8-w cochlea of $Cx26^{R75W+}$ mouse constructed with 3D graphics software IMARIS (Carl Zeiss). Conformation of GJPs in a 8-w cochlea of $Cx26^{R75W+}$ mouse with the control littermate (non-Tg) constructed with 3D graphics software IMARIS (Carl Zeiss). Three-dimensional video images were constructed from z-stacked confocal images to show the detailed GJP formations and the whole structure of ISCs by the labeling of Cx30 (red) and DAPI (light blue). This video is a diagram to show the difference of GJP size in $Cx26^{R75W+}$ mouse and the control littermate (non-Tg).

Supplemental Video 2

Conformation of GJPs in **a** 3-w cochlea of $Cx26^{f/f}$P0Cre mouse constructed with 3D graphics software IMARIS (Carl Zeiss). About 1.6 % of the ISCs had Cx26 expression on at least one lateral side (Figure 3), and these cells showed partial cellular mosaicism in $Cx26^{f/f}$P0Cre mice. Constructed three-dimensional video revealed that each lateral side of the cell junctions could be clearly distinguished as large, flat GJPs with Cx26 (red) and Cx30 (green) or as fragmented, small GJP vesicles with Cx30 alone at 3 w.

Supplemental Video 3

Conformation of GJPs in **a** 3-w cochlea of $Cx26^{f/f}$P0Cre mouse constructed with 3D graphics software IMARIS (Carl Zeiss). A high-magnification video of **Supplementary Video S2** showing the GJPs composed of Cx30 (green) with or without Cx26 (red) at the region of the cellular mosaicism.

Supplemental Video 4

Ca^{2+} imaging in developing cochlear tissue (Control, low magnification). Cochlear tissue from a P5 control mouse was loaded with the Ca^{2+} reporter fluo-4 acetoxymethyl ester (AM). Video images were taken at 1 frame/500 ms for 7 min.

Supplementary Video 5

Ca^{2+} imaging in developing cochlear tissue ($Cx26^{f/f}$P0Cre, low magnification). Cochlear tissue from a P5 $Cx26^{f/f}$P0Cre mouse was loaded with the Ca^{2+} reporter fluo-4 AM. Video images were taken at 1 frame/500 ms for 7 min.

Supplemental Video 6

Ca^{2+} imaging in developing cochlear tissue (Control, high magnification). Cochlear tissue of a P5 control mouse was loaded with the Ca^{2+} reporter fluo-4 AM. Video images were taken at 1 frame/500 ms for 7 min.

Supplemental Video 7

Ca^{2+} imaging in developing cochlear tissue ($Cx26^{f/f}$P0Cre, high magnification). Cochlear tissue from a P5 $Cx26^{f/f}$P0Cre mouse was loaded with the Ca^{2+} reporter fluo-4 AM. Video images were taken at 1 frame/500 ms for 7 min.

Supplemental methods

Auditory brainstem response (ABR)

All electrophysiological examinations were performed within an acoustically and electrically insulated and grounded test room. Mice ranging in age from P10 to P14 were studied. For ABR measurement, stainless-steel needle electrodes were placed at the vertex and ventrolateral to the left and right ears. The ABR was measured using waveform storing and stimulus control of the Scope software from the Power Laboratory system (model PowerLab4/25; AD Instruments), and electroencephalogram recording was made with an extracellular amplifier AC PreAmplifier (model P-55; Astro-Med). Acoustic stimuli were delivered to the mice through a coupler type speaker (model ES1spc; Bio Research Center). The threshold was determined for frequencies of 8 and 20 kHz from a set of responses at varying intensities with 5-dB intervals, and electrical signals were averaged at 512 repetitions. The maximum output level was 93.5 and 83.4 dB at 8 and 20 kHz, respectively, and 5 dB was added to these values when the ABR was not detected in the maximum output for statistical analysis.

Ca^{2+} imaging

The propagation of spontaneous Ca^{2+} transients via gap junctions in developing cochleae was recorded using the Ca^{2+} indicator fluo-4 as described [1]. Sequential fluorescence images were

acquired using a Nipkow disc confocal system (CSU22, Yokogawa, Japan) and AQUACOSMOS software (Hamamatsu Photonic), and analyzed with ImageJ software (NIH). Signals were expressed as relative changes in fluorescence emission intensity ($\Delta f/f_0$), where f_0 is the initial (pre-stimulus) fluorescence, f is the post-stimulus fluorescence at time t and $\Delta f = f - f_0$. All live-cell imaging experiments were performed at room temperature (24–26°C). The images were processed and analyzed with NIH ImageJ software, and the mean propagation range of the Ca^{2+} was measured and compared using Student's *t*-test (Microsoft Excel).

Co-immunoprecipitation

Co-immunoprecipitation of Cx26-containing macromolecular complexes was performed using Dynabeads Co-Immunoprecipitation Kit (Life technologies, Carlsbad, CA). Briefly, magnetic beads (Dynabeads® M-270 Epoxy, Life technologies, Carlsbad, CA) were conjugated to anti-Cx26 rabbit IgG (Life technologies, Carlsbad, CA) and were incubated with protein lysates obtained from six cochleae for 30 min at 4°C. The protein complexes were then eluted and detected by western blotting.

Exogenous overexpression of Cx26 in cochlear organotypic cultures transduced with AAV

To overexpress Cx26 in cochlear organotypic cultures, AAV vector containing the human Cx26 tagged with FLAG under the control of the CMV promoter was generated. The coding region of human *GJB2* cDNA (GenBank accession number NM_004004) was inserted into

pAAV-IRES-hrGFP vector (Agilent Technologies). This AAV-Cx26-FLAG vector was applied to cochlear organotypic cultures obtained from 6-week-old mouse inner ears and was incubated for 72 h. The cochlear organotypic cultures were obtained as previously described (25: Anselmi et al. PNAS 2008 vol.105 (48) 18770-75) from 6-week-old mouse inner ears from 4 mice (4 cochleae). These were fixed in 4% paraformaldehyde and immunolabeled with Anti-FLAG® M2 mouse monoclonal antibody (Sigma-Aldrich, St. Louis, MO). Fluorescence confocal images were obtained with a LSM510-META confocal microscope (Carl Zeiss, Jena, Germany). The GJP sizes represented by this immunolabeling were measured by LSM Image Browser (Carl Zeiss) and compared using Student's *t*-test (Microsoft Excel).